nature communications

Article

https://doi.org/10.1038/s41467-025-62615-y

Genome-wide in vivo CRISPR screens identify GATOR1 complex as a tumor suppressor in Myc-driven lymphoma

Received: 30 October 2024

Accepted: 28 July 2025

Published online: 21 August 2025

Check for updates

Margaret A. Potts[1,2,3,15], Shinsuke Mizutani[1,2,10,15], Yexuan Deng[1,2,3,4,15], Srimayee Vaidyanathan[5,6,11], Keziah E. Ting[5,6], Göknur Giner[1,2,3], Shruti Sridhar[7], Girija Shenoy[7], Yang Liao[3,8,12], Sarah T. Diepstraten[1,2], Andrew J. Kueh[1,2,3,8], Martin Pal[1,2,13], Geraldine Healey[1,3], Lin Tai[1,3], Zilu Wang[1,2,14], Christina König[1,3], Deeksha Kaloni[1,2], Lauren Whelan[1], Michael J. G. Milevskiy[1,2], Hannah D. Coughlan[1,2], Giovanna Pomilio[1,5], Andrew H. Wei[1,5], Jane E. Visvader[1,2], Anthony T. Papenfuss[1,2], Stephen Wilcox[1,2], Anand D. Jeyasekharan[7], Wei Shi[3,8,12], Emily J. Lelliott[1,2,3,8], Gemma L. Kelly[1,2], Kristin K. Brown[5,6,9,16], Andreas Strasser[1,2,16] ✉ & Marco J. Herold[1,2,3,8,16] ✉

Identifying tumor suppressor genes is predicted to inform on the development of novel strategies for cancer therapy. To identify new lymphoma driving processes that cooperate with oncogenic MYC, which is abnormally highly expressed in ~70% of human cancers, we use a genome-wide CRISPR gene knockout screen in *Eμ-Myc;Cas9* transgenic hematopoietic stem and progenitor cells in vivo. We discover that loss of any of the GATOR1 complex components - NPRL3, DEPDC5, NPRL2 - significantly accelerates c-MYC-driven lymphoma development in mice. MYC-driven lymphomas lacking GATOR1 display constitutive mTOR pathway activation and are highly sensitive to mTOR inhibitors, both in vitro and in vivo. These findings identify GATOR1 suppression of mTORC1 as a tumor suppressive mechanism in MYC-driven lymphomagenesis and suggest an avenue for therapeutic intervention in GATOR1-deficient lymphomas through mTOR inhibition.

Abnormally high expression of oncogenic *MYC* is observed in ~70% of human cancers, highlighting it as an attractive therapeutic target[1]. However, to date no MYC directed therapeutics have been successfully developed. Therapeutic targeting of MYC is challenging for many reasons, including its involvement in regulating many essential cellular processes, such as cell cycling, proliferation, differentiation, metabolism and cell death[2]. Therefore, understanding which processes are critical for MYC-driven oncogenesis might reveal downstream druggable cancer dependencies.

To identify genes that suppress MYC-driven cancer, we conducted an unbiased genome-wide CRISPR/Cas9 gene knockout screen in vivo. We employed the *Eμ-Myc* transgenic mouse model, a well-accepted pre-clinical model of Burkitt Lymphoma (BL). These transgenic mice were engineered such that murine c-Myc is constitutively expressed at high levels throughout B cell development under the control of the mouse *Eμ* enhancer. Consequently, this induces a partial differentiation block and increased proliferation of early B cell progenitors that amass as a pool of pre-leukemic cells[3,4]. These pre-leukemic cells are prone to undergoing apoptosis, and spontaneous acquisition of additional cooperating mutations enables malignant transformation into monoclonal surface Ig$^-$ pre-B or surface Ig$^+$ B-cell lymphomas that disseminate to all hematopoietic organs with mice succumbing to disease with a median survival of ~110 days[5].

A full list of affiliations appears at the end of the paper. ✉e-mail: strasser@wehi.edu.au; marco.herold@onjcri.org.au

While genome-wide CRISPR/Cas9 screening approaches are feasible in vitro using immortalized or other easily transducible cell lines, they do not accurately model the complexities of cancer initiation or metastasis, nor response to therapies, or interactions within the tumor microenvironment[6,7]. Previously, only few in vivo CRISPR/Cas9 screens have employed non-transformed cells to interrogate cancer initiation[8–10]. Moreover, most such in vivo screens exploring tumorigenesis were performed either with small focused sgRNA[11,12] or siRNA[13] libraries, thereby limiting the hit identification to known cellular signaling pathways. Other screens employed genome-wide targeting, but utilized transplantation of established cancer cell lines, which possess complex (and possibly confounding) genetic aberrations, rather than primary cells[14–18].

Here, we conducted an unbiased genome-wide CRISPR/Cas9 knockout screen in primary cells in vivo to identify tumor suppressor genes whose loss cooperates with over-expression of MYC in driving lymphomagenesis. Primary *Eμ-Myc;Cas9* double transgenic hematopoietic stem and progenitor cells (HSPCs) that were transduced with a genome-wide sgRNA library were transplanted into lethally irradiated recipient mice. The transplanted HSPCs can reconstitute all blood compartments while also being predisposed to developing lymphoma, whereby CRISPR/Cas9 deletion of a tumor suppressor gene would accelerate malignant transformation compared to lymphoma development without such an oncogenic lesion. Since lymphomas in the *Eμ-Myc* transgenic model are monoclonal[5], our screen was designed to identify the most powerful tumor suppressor pathways as each manipulated *Eμ-Myc* transgenic HSPC deleted for one gene and transplanted into a recipient mouse will have to compete with thousands of other genetically manipulated *Eμ-Myc* transgenic HSPCs, resulting in the selection of the strongest hit in each recipient mouse.

Aberrations in regulators of the cell death pathway are well known to cooperate with over-expression of c-Myc in lymphomagenesis[19–26]. This was evident by the observation that deletion of the tumor suppressor gene p53 was the most frequent hit in our screen. However, several top hits in our screen were genes encoding negative regulators of the mTORC1 pathway, which coordinates cellular metabolism to support cell growth, survival and proliferation[27]. Two components of the mTORC1 inhibitory complex GATOR1 were top hits, and they were not previously described as suppressors of Myc-driven lymphomagenesis. We revealed the importance of this negative regulator of cell metabolism for tumor suppression, including in human B cell lymphoma through analysis of human cancer genome databases. Of note, we show that lymphomas driven by Myc over-expression and loss of GATOR1 are highly sensitive to single agent mTOR inhibitor treatment. This suggests a therapeutic strategy for Myc-driven lymphomas that has defects in GATOR1 function.

Results

Genome-wide in vivo CRISPR/Cas9 gene knockout screen identifies mTOR inhibitory pathway components as potent suppressors of MYC-driven lymphomagenesis

Previously our laboratory conducted an RNA interference (RNAi) screen where the shRNA library was focused on p53 regulated genes[13]. To identify previously unknown suppressors of Myc-driven lymphomagenesis beyond the p53 pathway, we performed an unbiased genome-wide CRISPR/Cas9 gene knockout screen in vivo. Specifically, fetal liver cells (FLCs), an abundant source of HSPCs with the capacity to reconstitute all hematopoietic cell types, from C57BL/6-Ly5.2 *Eμ-Myc;Cas9* double transgenic day (E)13.5 mouse embryos were transduced ex vivo with a pooled whole-genome sgRNA library. The library contains 87,987 sgRNAs targeting 19,150 mouse protein coding genes (4-5 sgRNAs per gene)[28]. A transduction efficiency of 20-30% was achieved, as determined by flow cytometric analysis of the blue fluorescent protein (BFP) tag expression. This level of library transduction engenders a relatively low likelihood of co-transducing multiple sgRNAs into a single FLC. At 24 h post-transduction, the FLCs were transplanted intravenously into lethally irradiated (ablating the host hematopoietic compartment) congenic C57BL/6-Ly5.1 recipient mice (Fig. 1A). As a positive control, *Eμ-Myc;Cas9* FLCs were transduced with a sgRNA targeting mouse *p53* (*sgp53*), as loss of *p53* is known to substantially accelerate MYC-driven lymphomagenesis[29]. As a negative control, *Eμ-Myc;Cas9* FLCs were transduced with a sgRNA targeting the human *BIM* gene that has no predicted activity in the mouse genome (*sgControl*). Recipient mice transplanted with *sgControl* transduced FLCs developed lymphoma with a median latency of ~140 days post-transplantation, while recipients transplanted with *sgp53* transduced FLCs exhibited significantly accelerated lymphoma development (median latency of ~25 days) (Fig. 1B), consistent with a previous report[30]. Notably, several mice transplanted with sgRNA library-transduced FLCs developed lymphoma considerably earlier (median latency ~74 days) than the mice transplanted with *sgControl* transduced FLCs (Fig. 1B). This indicates that these accelerated lymphomas contained sgRNAs that led to the deletion of genes involved in the suppression of Myc-driven lymphomagenesis. All recipients transplanted with *Eμ-Myc;Cas9* FLCs, regardless of the sgRNA used for transduction or ethical endpoint, presented with sIg^- pre-B lymphoma or sIg^+ B cell lymphoma (Supplementary Fig. S1A–B), as expected in this model[5].

To identify the sgRNAs that caused accelerated lymphomagenesis, we conducted next generation sequencing (NGS) on genomic DNA (gDNA) extracted from the spleens of mice transplanted with sgRNA library-transduced FLCs that developed lymphoma prior to 75 days after reconstitution (arbitrary cut-off for accelerated lymphoma chosen; $n = 59$ from 113 transplanted mice) (Fig. 1B). Because *Eμ-Myc* lymphomas are monoclonal, we expected one sgRNA to be selected for and thus be dominant in each lymphoma sample by sequencing. However, analysis of gDNA from each whole spleen, which contains not only malignant lymphoma cells but also non-malignant hematopoietic cells (e.g., nucleated erythroid and myeloid cells) often revealed up to 4 dominant sgRNAs accounting for a large proportion of the sequencing counts (Supplementary Fig. S2 and Supplementary Data 1). This may be due to incidental co-transduction of more than one sgRNA into one HSPC that proceeded to transform into lymphoma. Alternatively, this may be due to relatively low lymphoma burden within the spleen with substantial presence of non-malignant hematopoietic cells that can also contain sgRNAs that had been transduced in the HSPCs that gave rise to these cells. Therefore, hits that may target candidate tumor suppressor genes were prioritized according to meeting one or more of the following criteria: (i) the sgRNA was the dominantly represented sgRNA within a lymphoma containing sample, (ii) a sgRNA for one gene was identified in more than one lymphoma sample and was amongst the three most dominantly represented sgRNAs, and (iii) more than one sgRNA for that gene was identified in multiple independent lymphoma samples (Fig. 1C, and Supplementary Fig. S2 and Fig. S3A). In addition, we observed low read counts of numerous sgRNAs collectively targeting more than 75% of all genes. These sgRNAs likely conferred no selection pressure and were present in the non-malignant hematopoietic cells within the spleen samples from the FLC transplanted recipient mice (Supplementary Fig. S2 and Fig. S3B–F). This provides an important internal control to demonstrate high-level sgRNA library representation in each reconstituted mouse. In fact, 809 (~ 4%) of genes for which no sgRNA was represented are considered essential genes according to DepMap and the TCGA, and therefore would not be expected to be represented in hematopoietic cells from the reconstituted mice[31]. Collectively, these data indicate comprehensive gene coverage of the genome-wide sgRNA library that is usually significantly reduced following transplantation into mice[14].

Overall, 38 hits were identified from the 59 lymphoma samples sequenced. Some gene hits were identified in multiple lymphomas,

https://doi.org/10.1038/s41467-025-62615-y

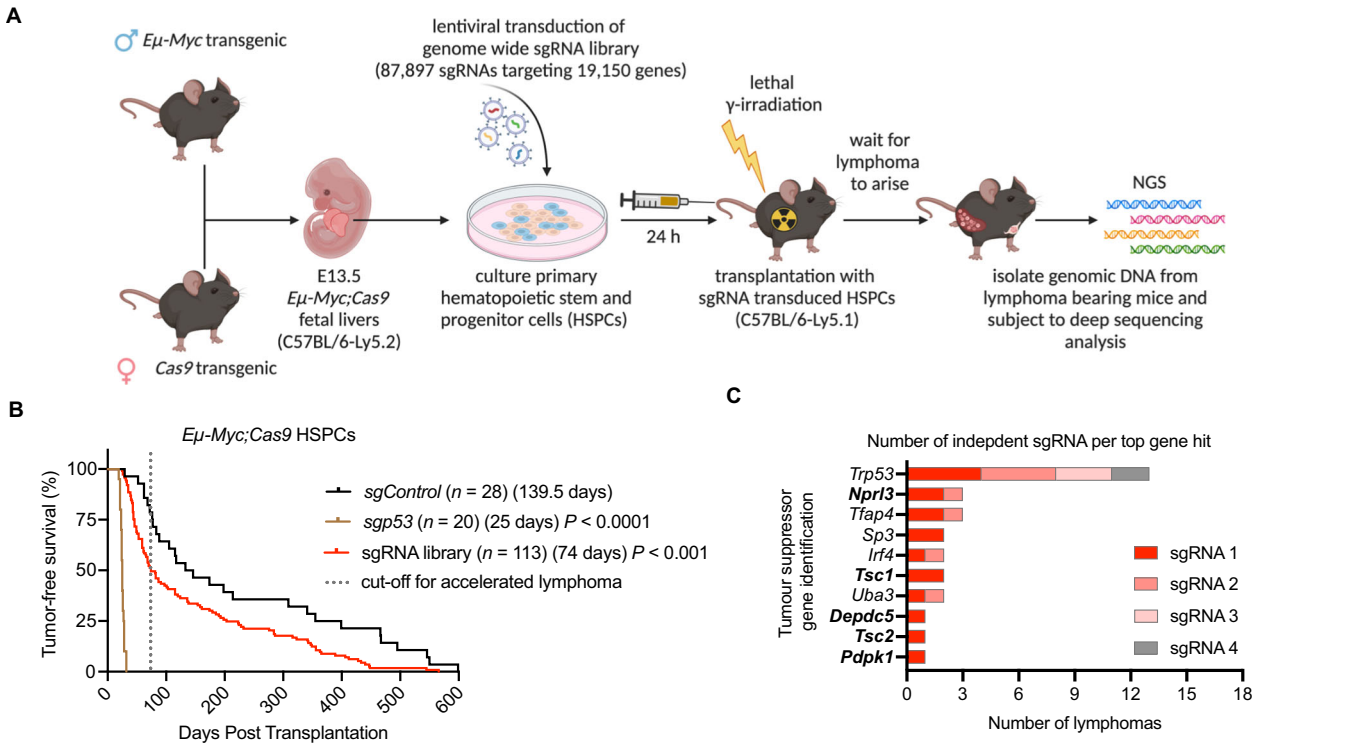

Fig. 1 | In vivo genome-wide CRISPR/Cas9 gene knockout screen identifies candidate tumor suppressors. A Schematic of the experimental strategy for performing in vivo genome-wide sgRNA screens to identify candidate tumor suppressors. Fetal liver cells (FLCs), a rich source of hematopoietic stem/progenitor cells (HSPCs), from E13.5 *Eμ-Myc;Cas9* embryos (C57BL/6-Ly5.2 background) were transduced with lentiviruses containing sgRNAs targeting *p53* (*sgp53;* positive control), a negative control sgRNA targeting human *BIM* (*sgControl)* or a whole-genome sgRNA library [28]. The transduced FLCs were injected intravenously (i.v.) into lethally irradiated (2 × 5.5 Gy, 3 h apart) congenic recipient C57BL/6-Ly5.1 mice. Lymphoma bearing mice displayed enlarged spleen, lymph nodes and/or thymus. Genomic DNA was isolated from the spleen, comprising mostly of lymphoma cells but also containing non-transformed hematopoietic cells. The enriched sgRNAs were identified by NGS. Schematic created in BioRender. Potts, M. (https://BioRender.com/smdpt7f). **B** Tumor-free survival of mice transplanted with *Eμ-Myc;Cas9* FLCs that had been lentivirally transduced with the positive control sgRNA (*sgp53)*, the negative control sgRNA (*sgControl)* or a whole-genome sgRNA library. The dotted line represents cut-off for lymphomas from the whole genome sgRNA library cohort that were arbitrarily deemed to be accelerated and therefore selected for further analysis. *n* represents total number of transplanted mice per sgRNA from 6 reconstitution cohorts. Median survival is indicated in brackets. Log-rank (Mantel-Cox) statistical test for survival curve comparison to *sgControl*. **C** Top 10 tumor suppressor genes identified as hits, determined by frequency of their sgRNAs detected in independent lymphomas from mice from the whole-genome sgRNA library cohort that showed accelerated lymphoma, with the corresponding sgRNAs found to be highly enriched (> 50% of reads within a given lymphoma) by sequencing. Genes emboldened (five of the top 10) represent those encoding proteins with functions in the mTORC1 inhibitory pathway. Source data provided as Supplementary Data 1 and as Source Data File.

either through repeated detection of the same sgRNA or multiple distinct sgRNAs targeting the same gene. Of note, some of these sgRNAs target known tumor suppressor genes. The most prominent hit was *p53*, with four of the five sgRNAs targeting *p53* being the dominant sgRNA detected in 13 different lymphomas (Fig. 1C, Supplementary Fig. S2 and Fig. S3A). Notably, the screen also identified new candidate tumor suppressor genes, such as *Tfap4*, where two distinct sgRNAs were dominant in three lymphomas. This hit was validated and the function of TFAP4 was investigated in a separate study[32]. Pathway analysis of the top gene hits using the DAVID Bioinformatics tool revealed that five of the top gene hits - *Nprl3*, *Depdc5*, *Tsc1*, *Tsc2* and *Pdpk1*- function in the mTOR signaling pathway[33,34]. Among these hits, *Nprl3* (with two distinct sgRNAs dominant in three lymphomas) and *Depdc5* (with one sgRNA dominant in one lymphoma) (Fig. 1C, and Supplementary Fig. S2 and Fig. S3A) were particularly interesting as they both encode essential components of the GATOR1 complex that negatively regulates mTORC1 in response to amino acid availability[27]. While one study identified loss of function mutations in the GATOR1 complex components in some solid malignancies[35], GATOR1 has not previously been reported to suppress Myc-driven hematological malignancies. In contrast, the top hits Tuberous sclerosis complex 1 (*Tsc1*) and 2 (*Tsc2*), which also negatively regulate mTORC1, but in response to growth factor signaling, have previously been implicated in the suppression of Myc-driven lymphoma development[27,36,37]. These findings indicate that our unbiased in vivo CRISPR gene knockout screening approach successfully selected for the most potent suppressors of Myc-driven lymphoma development, identifying both known (e.g., *p53*) and unknown (e.g., *Nprl3*, *Depdc5*) tumor suppressor genes. We found that the mTOR inhibitory GATOR1 pathway plays a previously underappreciated critical role in Myc-driven lymphoma development as sgRNAs targeting genes encoding two components of this complex outcompeted sgRNAs against most other genes.

Loss of any GATOR1 complex component accelerates Myc-driven lymphoma development

The GATOR1 complex is composed of three subunits, NPRL3, DEPDC5, and NRPL2 (Fig. 2A), that are all required for its function[38]. While *Nprl3* and *Depdc5* were identified as hits in our screen, the third component *Nprl2* was not a hit. Although sgRNAs targeting *Nprl2* were represented in the screen, they were detected at very low abundance in the sequencing read counts from the lymphoma of one sgRNA library recipient mouse, in which *p53* was the dominant hit. Hence loss of *p53* was more strongly selected for than loss of *Nprl2*. However, since all three GATOR1 complex subunits are required for its function, we

https://doi.org/10.1038/s41467-025-62615-y

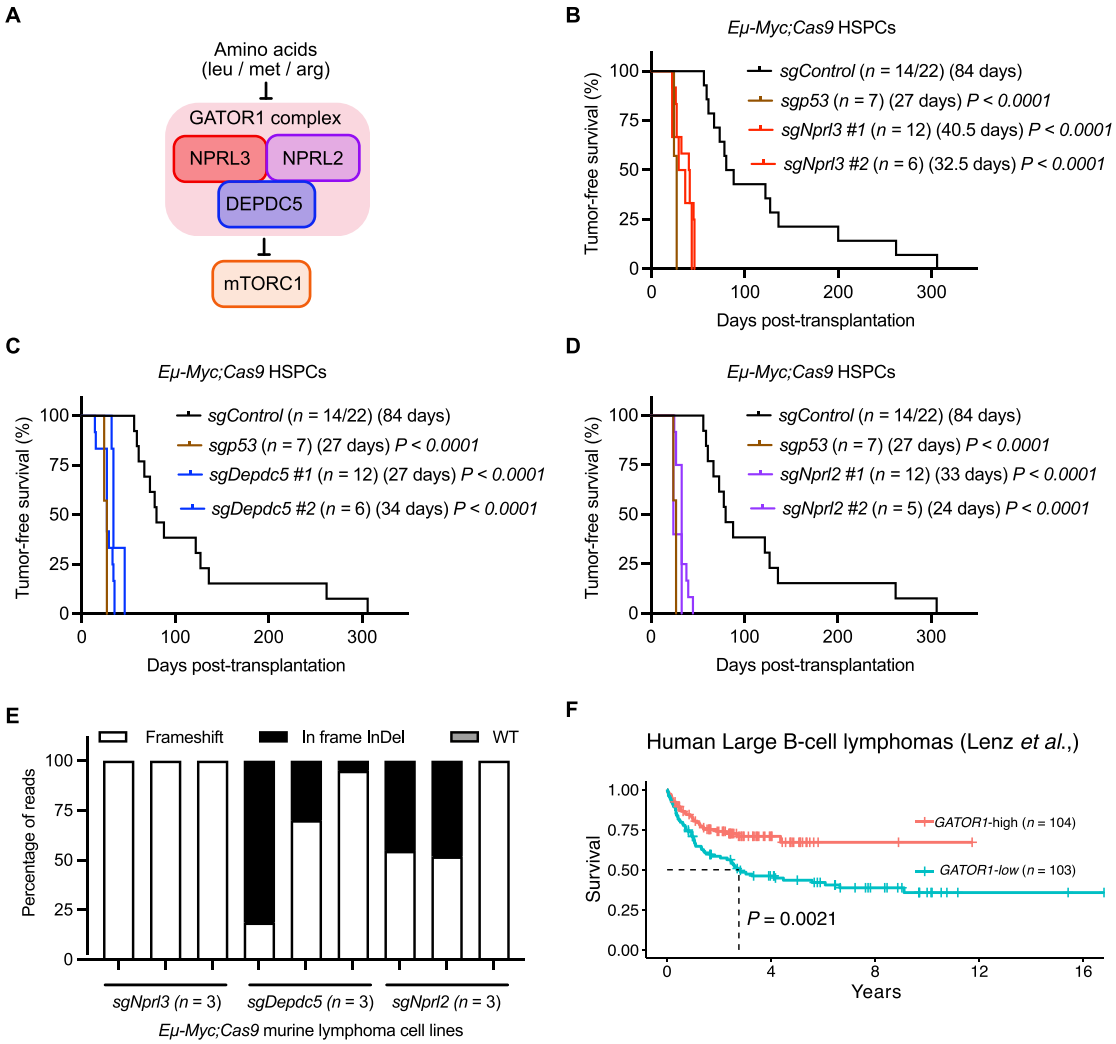

Fig. 2 | Validation of GATOR1 complex components as suppressors of Myc-driven lymphomagenesis in mice as well as in human MYC-driven lymphomas. **A** Schematic of the GATOR1 complex, consisting of three proteins, NPRL3, DEPDC5 (sgRNAs targeting their genes identified as hits in our genome-wide CRISPR screen), and NPRL2. The GATOR1 complex negatively regulates mTORC1 signaling in response to the availability of the amino acids leucine (Leu), methionine (Met) and arginine (Arg). **B**–**D** Tumor-free survival of mice transplanted with FLCs from *Eμ-Myc;Cas9* E13.5 embryos that had been transduced with either the sg*p53* (positive control), the negative control sgRNA (*sgControl*) or two independent sgRNAs each for targeting either *Nprl3* (**B**) *Depdc5* (**C**) or *Nprl2* (**D**). *n* represents the number of transplanted mice per sgRNA across two transplanted mouse cohorts. Median survival is indicated in brackets. Two-sided log-rank (Mantel-Cox) test was used for comparison of mouse survival curves to *sgControl*. **E**, Proportions of frameshift, in frame InDels or wildtype (wt) sequence reads for the target gene of each sgRNA, analyzed by NGS. Each bar represents one lymphoma cell line derived from lymphomas of recipient mice that had been transplanted with *sgNrpl3, sgDepdc5* or *sgNprl2 Eμ-Myc;Cas9* FLCs ($n = 3$ cell lines per genotype). Source data provided as Supplementary Data 2. **F** Survival of human patients with diffuse large B cell lymphoma (DLBCL)[39], a cancer driven by abnormally high *c-MYC* expression, stratified by *GATOR1* mRNA expression, where the *GATOR1*-low ($n = 103$) strata is defined as expression of either the *NPRL3, DEPDC5* or *NPRL2* mRNA in the lowest quartile. The others were grouped into the *GATOR1*-high strata ($n = 104$). Two-sided log-rank Kaplan-Meier statistical test, $P = 0.0021$. Source data are provided as a Source Data file.

decided to evaluate the potential of each component to accelerate Myc-driven lymphomagenesis. To this end, two independent sgRNAs targeting each of *Nprl3* (*sgNprl3*), *Depdc5* (*sgDepdc5*) and *Nprl2* (*sgNprl2*), were individually introduced into FLCs from *Eμ-Myc;Cas9* E13.5 embryos that were then transplanted into lethally irradiated C57BL/6-Ly5.1 congenic recipient mice. Strikingly, all sgRNAs targeting *Nprl3*, *Depdc5* or *Nprl2* significantly accelerated c-MYC-driven lymphomagenesis to a similar extent as each other, and their impact was in fact comparable to that of sgRNAs targeting the potent tumor suppressor p53 (sg*p53*) (Fig. 2B–D). As expected in the *Eμ-Myc* transgenic mouse model[5], all transplanted mice regardless of the sgRNA or time of lymphoma onset presented with enlarged hematopoietic tissues and elevated white blood cell counts at ethical endpoint (Supplementary Fig. S4A–C). Efficient deletion of *Nprl3*, *Depdc5* or *Nprl2* by CRISPR/Cas9 was confirmed by targeted gene sequencing of gDNA isolated from cell lines derived from these lymphomas (Fig. 2E, and Supplementary Data 2). These findings reveal that loss of any GATOR1 complex component is sufficient to abrogate its tumor suppressive function and thereby markedly accelerate MYC-driven lymphoma development.

To examine if these findings are relevant to human cancer, we analyzed B cell lymphoma patient cohorts. Nine independent B cell lymphoma patient cohorts with gene expression profiles and clinical characteristics were analyzed, stratifying patients by the levels of *GATOR1* component mRNA expression and *MYC* mRNA expression (Supplementary Table 1). In only one patient dataset of diffuse large B cell lymphoma (DLBCL) patient samples (Lenz et al.)[39], we observed that *GATOR1*-low expression (defined as *NPRL3, DEPDC5* or *NPLR2* mRNA expression in the bottom 25%, $n = 103$ patients) is associated with

https://doi.org/10.1038/s41467-025-62615-y

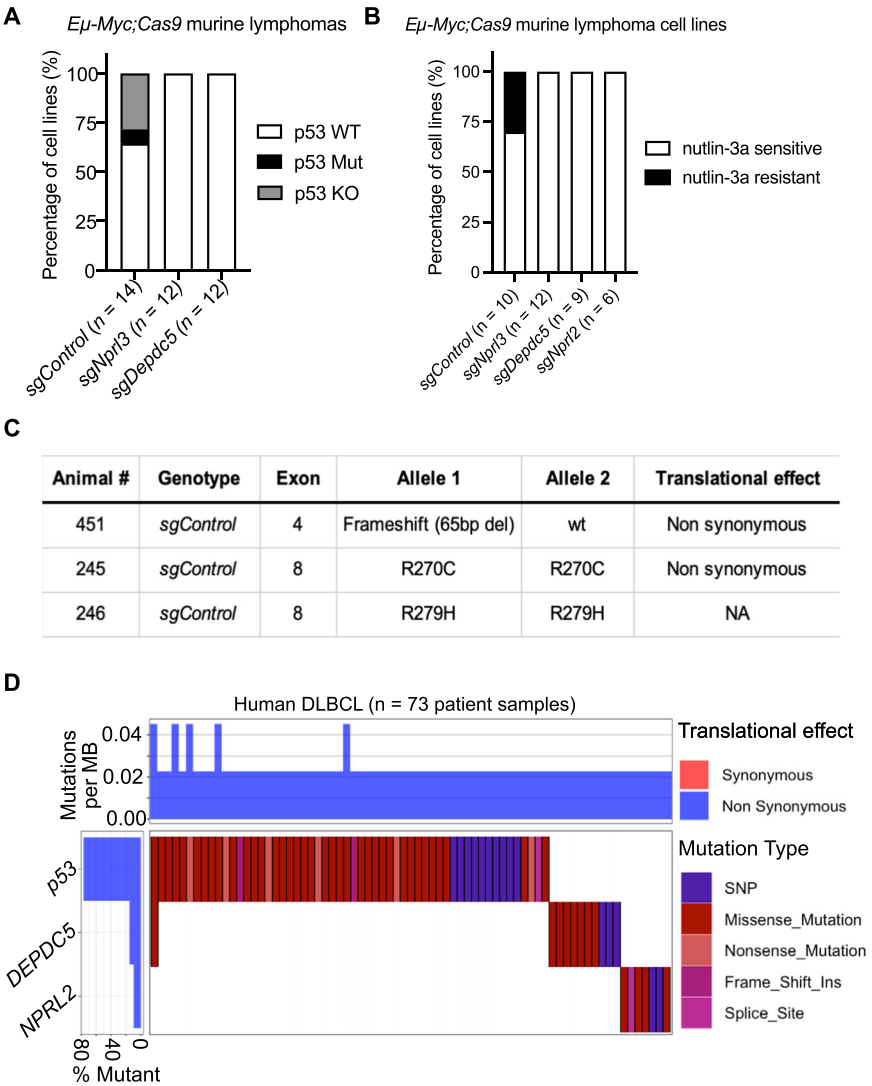

C

Animal #	Genotype	Exon	Allele 1	Allele 2	Translational effect
451	*sgControl*	4	Frameshift (65bp del)	wt	Non synonymous
245	*sgControl*	8	R270C	R270C	Non synonymous
246	*sgControl*	8	R279H	R279H	NA

Fig. 3 | GATOR1 deficiency obviates the pressure to lose p53 function during Myc-driven lymphomagenesis. A Summary graph of Western blot analyses showing proportions of *sgControl*, *sgDepdc5* or *sgNprl3* Eμ-*Myc;Cas9* lymphomas that are p53 wt, p53 mutant (Mut) or p53 knockout (KO). *n* = number of lymphomas from each genotype analyzed, indicated below the bars. **B** Summary plot showing the proportions of nutlin-3a sensitive (p53 wt) or nutlin-3a resistant (p53 function defective) *Eμ-Myc;Cas9* lymphoma cell lines for each genotype. **C** Next generation sequencing of exons 4-11 of the *p53* genomic locus to identify mutations. 3/10 *sgControl*, 0/9 *sgNprl3*, 0/8 *sgDepdc5* and 0/7 *sgNprl2* Eμ-*Myc;Cas9* lymphoma cell lines tested carried mutations in the *p53* gene. Source data provided as Supplementary Data 3. Predicted translational effect of the equivalent human homologue mutation according to the TP53 database (accessed: https://tp53.cancer.gov/). 'NA' means 'unknown' effect. **D** Mutual exclusivity mutational analysis of *TP53 (p53)* and the GATOR1 component genes *DEPDC5* and *NPRL2* in human DLBCL patient samples[43–45]. Translational effect of mutation indicated, where synonymous refers to silent mutations and non-synonymous mutations cause an amino acid change. *n* = 73 patient samples, $P < 0.0001$ using two-sided Fisher's exact test. Source data are provided as a Source Data file.

significantly poorer survival of patients compared to those with *GATOR1*-high expression (*n* = 104 patients) (Fig. 2F). The rationale for this sample stratification is that GATOR1 function is impaired when it lacks any one of its three components. Within this same DLBCL cohort, significantly poorer survival of patients was also observed when patients were stratified into *MYC*-high expression (defined as *MYC* mRNA expression above the mean) and *GATOR1*-low expression compared to *MYC*-high and *GATOR1*-high stratified patients (Supplementary Table 1). While this is observed in one patient cohort, hinting that GATOR1 complex gene expression is associated with poorer B cell lymphoma patient outcomes, more analysis is required to strengthen this finding.

Loss of GATOR1 obviates the pressure for p53 mutation in Myc-driven lymphomagenesis

Given that deletion of GATOR1 components accelerates lymphomagenesis to a similar extent as p53 deletion and since Myc-lymphomas are prone to select for aberrations in the p53 pathway, we examined p53 mutational status and function in *sgControl* and GATOR1-deficient *Eμ-Myc* lymphomas. Consistent with previous reports that spontaneous mutations in p53 are selected for in ~30% of *Eμ-Myc* lymphomas[20,23], we found that ~30% of *sgControl* lymphomas had acquired p53 pathway defects. This was evidenced by expression of stabilized mutant p53 protein and/or high levels of downstream $p19^{ARF}$, which is increased when p53 function is lost[20,23,40] (Fig. 3A, and Supplementary Fig. S5A). In contrast, no such abnormalities in p53 or $p19^{ARF}$ were observed in the 24 GATOR1-deficient *Eμ-Myc;Cas9* lymphomas (Fig. 3A, and Supplementary Fig. S5A). To functionally validate these findings, we treated lymphoma cell lines in culture with nutlin-3a, which induces apoptotic cell death in a p53-dependent manner[41,42]. Three out of 10 *sgControl Eμ-Myc;Cas9* lymphoma cell lines were resistant to nutlin-3a, consistent with the predicted presence of mutations in p53, whereas 100% of GATOR1-deficient lymphoma cell

lines were highly sensitive to nutlin-3a, indicating the presence of functional wildtype (wt) p53 and intact downstream pathways ($n = 27$; Fig. 3B, Supplementary Fig. S5B). NGS confirmed that the three nutlin-3a resistant *sgControl Eμ-Myc;Cas9* lymphomas had indeed acquired pathologic *p53* mutations, whereas all 27 (100%) GATOR1-deficient *Eμ-Myc;Cas9* lymphomas maintained wt *p53* status (Fig. 3C, and Supplementary Data 3). Extending this analysis to independent cohorts of human DLBCL patient samples[43–45], 11/73 (~15%) harbored non-synonymous mutations in *DEPDC5* and 9/73 (~12%) harbored non-synonymous mutations in *NPRL2* (Fig. 3D). Mutational data on *NPRL3* were not available. All but one of these GATOR1 mutant human DLBCL samples carried wt *p53*, corroborating our findings in mice that mutations in *p53* and GATOR1 complex genes are mutually exclusive (Fig. 3D). Together, these data demonstrate that the GATOR1 complex is a potent suppressor of Myc-driven lymphomagenesis, obviating the pressure to also acquire mutations that disable the p53 pathway.

GATOR1 deficiency augments mTORC1 activity that can be diminished by direct inhibition of mTORC1

The GATOR1 complex is a well-known negative regulator of mTORC1. GATOR1 expression is suppressed if cytosolic concentrations of the specific amino acids leucine (Leu), methionine (Met) and arginine (Arg) are abundant[27]. We therefore hypothesized that lymphomas deficient in GATOR1 components would exhibit elevated phosphorylated S6 (phospho-S6), a surrogate marker of mTORC1 signaling, and fail to negatively regulate mTORC1 in response to amino acid starvation. Indeed, at steady state (in medium replete of amino acids and serum), we observed substantially higher levels of phospho-S6, indicative of increased mTORC1 activity in *Eμ-Myc;Cas9* lymphoma cells lacking *Nprl3* or *Depdc5* compared to *sgControl Eμ-Myc;Cas9* lymphoma cells (Fig. 4A–B). Even during culture in starvation medium (lacking all amino acids and serum)[38], phospho-S6 levels were higher in GATOR1-deficient *Eμ-Myc;Cas9* lymphoma cells compared to *sgControl Eμ-Myc;Cas9* lymphoma cells (Fig. 4B). This confirms the loss of GATOR1 function in these lymphoma cells, as amino acid starvation should activate the GATOR1 complex thereby inhibiting mTORC1 (Fig. 4A). Although the magnitude of phospho-S6 elevation in GATOR1-deficient *Eμ-Myc;Cas9* lymphoma cells above *sgControl* lymphomas, when cultured in starvation medium, was lower than that observed in steady state, this may be due to the actions of other amino acid sensors[46] dampening mTORC1 signaling in response to the lack of all amino acids and serum in the starvation medium, and thereby lowering phospho-S6 levels. Furthermore, deprivation of the amino acids that are uniquely sensed by the GATOR1 complex (Leu, Met, Arg) reduced phospho-S6 protein levels in control lymphomas (Fig. 4C; lane 3). In contrast, the GATOR1-deficient *Eμ-Myc;Cas9* lymphomas failed to inhibit mTORC1 following removal of these amino acids (Fig. 4C; lanes 7 and 11). Since GATOR1-deficient lymphomas displayed elevated mTORC1 activity, we considered whether inhibition of mTORC1 would restore signaling to normal levels. Notably, treatment with rapamycin, a compound that directly inhibits mTORC1 (Fig. 4A), markedly reduced the levels of phospho-S6 in *sgNprl3* and *sgDepdc5 Eμ-Myc;Cas9* lymphoma cells in both complete medium as well as in starvation medium lacking either all amino acids and serum or only the amino acids sensed by the GATOR1 complex specifically (Fig. 4B–C). These findings demonstrate that the loss of GATOR1 function drives constitutive mTORC1 activation in *Eμ-Myc* lymphomas.

GATOR1 deficiency perturbs cellular metabolism

Given that mTORC1 contributes to the regulation of multiple metabolic processes, we next explored changes in mTORC1 regulated metabolic pathways caused by loss of GATOR1 function. We performed RNA-Seq on *sgControl*, *sgNprl3* and *sgDepdc5 Eμ-Myc;Cas9* lymphoma cell lines following culture in either full serum medium (i.e. complete with 10% serum), or under starvation conditions (medium containing 1% serum). The latter condition reduces the impact of growth factor-mediated activation of mTORC1, which may obscure differential gene expression resulting from loss of GATOR1-mediated regulation of mTORC1. Differential gene expression in the context of GATOR1 deficiency was only observed in serum starvation conditions (Supplementary Fig. S6A–C). Therefore, further analysis was only performed on serum starvation dataset. This revealed marked overlap in the differentially expressed genes (DEGs) between *sgNprl3* and *sgDepdc5 Eμ-Myc;Cas9* lymphoma cells compared to *sgControl Eμ-Myc;Cas9* lymphoma cells (Supplementary Fig. S6D). While KEGG and GO pathway enrichment analyses did not reveal statistically significantly altered metabolic pathways, the GATOR1-deficient *Eμ-Myc;-Cas9* lymphoma cells displayed elevated expression of genes involved in mTORC1 regulated metabolic pathways, compared to the *sgControl Eμ-Myc;Cas9* lymphoma cells. This included genes involved in lipid/cholesterol biosynthesis, pentose phosphate pathway, one-carbon metabolism and the ATF4 transcription factor pathway which functions downstream of mTORC1 (Fig. 4D, Supplementary Fig. S6E). These findings demonstrate that GATOR1 deficiency promotes constitutive mTORC1 activation and renders lymphoma cells less sensitive to external factors that repress this pathway. Functional metabolic assays revealed no differences in mitochondrial function when comparing GATOR1-deficient lymphoma cells with control lymphoma cells (Supplementary Fig. S7A). However, consistent with known functions of mTORC1[27], we observed a trend towards elevated de novo lipogenesis in GATOR1-deficient lymphoma cells (Supplementary Fig. S7B), as well as increased incorporation of O-propargyl-puromycin (OPP) into nascent proteins, indicative of augmented translation capacity (Fig. 4E, and Supplementary Fig. S7C). Augmented translation of the pro-survival BCL-2 family member MCL-1, resulting from hyperactive mTORC1 via loss of TSC2, was reported to accelerate lymphomagenesis in *Eμ-Myc* transgenic mice[36]. However, GATOR1-deficient lymphoma cells had comparable mRNA gene expression levels of apoptotic family members as measured by RNA-Seq in 1% serum starvation, and comparable MCL-1 protein levels to *sgControl* lymphoma cells (Supplementary Fig. S7D). Moreover, MCL-1 protein expression was reduced similarly between *sgControl* and GATOR1-deficient *Eμ-Myc* lymphoma cells following treatment with rapamycin (Supplementary Fig. S7E). This indicates that loss of GATOR1-dependent regulation of mTORC1 does not accelerate Myc-driven lymphomagenesis by inhibiting cell death. This conclusion was supported by GATOR1-deficient lymphoma cells displaying no statistically significant difference in sensitivity to treatment with the MCL-1 inhibitor S63845[47] compared to sg*Control* lymphoma cells (Supplementary Fig. S7F). These results demonstrate that loss of GATOR1 promotes aberrant mTORC1 signaling, consequently providing metabolic advantages to lymphoma cells.

GATOR1-deficient lymphoma cells are highly sensitive to mTORC1 inhibition

As mTORC1 is constitutively activated in GATOR1-deficient lymphomas, we hypothesized that these cells might be “addicted” to a hyperactive mTORC1 pathway signalling, thereby potentially engendering a therapeutic vulnerability. Treatment with rapamycin (mTORC1 inhibitor) potently killed GATOR1-deficient cells in vitro, while *sgControl Eμ-Myc;Cas9* lymphoma cells were highly resistant to this treatment (Fig. 5A). Similarly, GATOR1-deficient lymphoma cells were sensitive to treatment with Torin1, a dual mTORC1 and mTORC2 inhibitor[48], whereas sg*Control Eμ-Myc;Cas9* lymphoma cells were only killed by very high doses of this agent that are not clinically relevant (Fig. 5B). Having demonstrated rapamycin sensitivity of *Eμ-Myc* lymphoma cells in vitro, we next assessed whether such treatment

https://doi.org/10.1038/s41467-025-62615-y

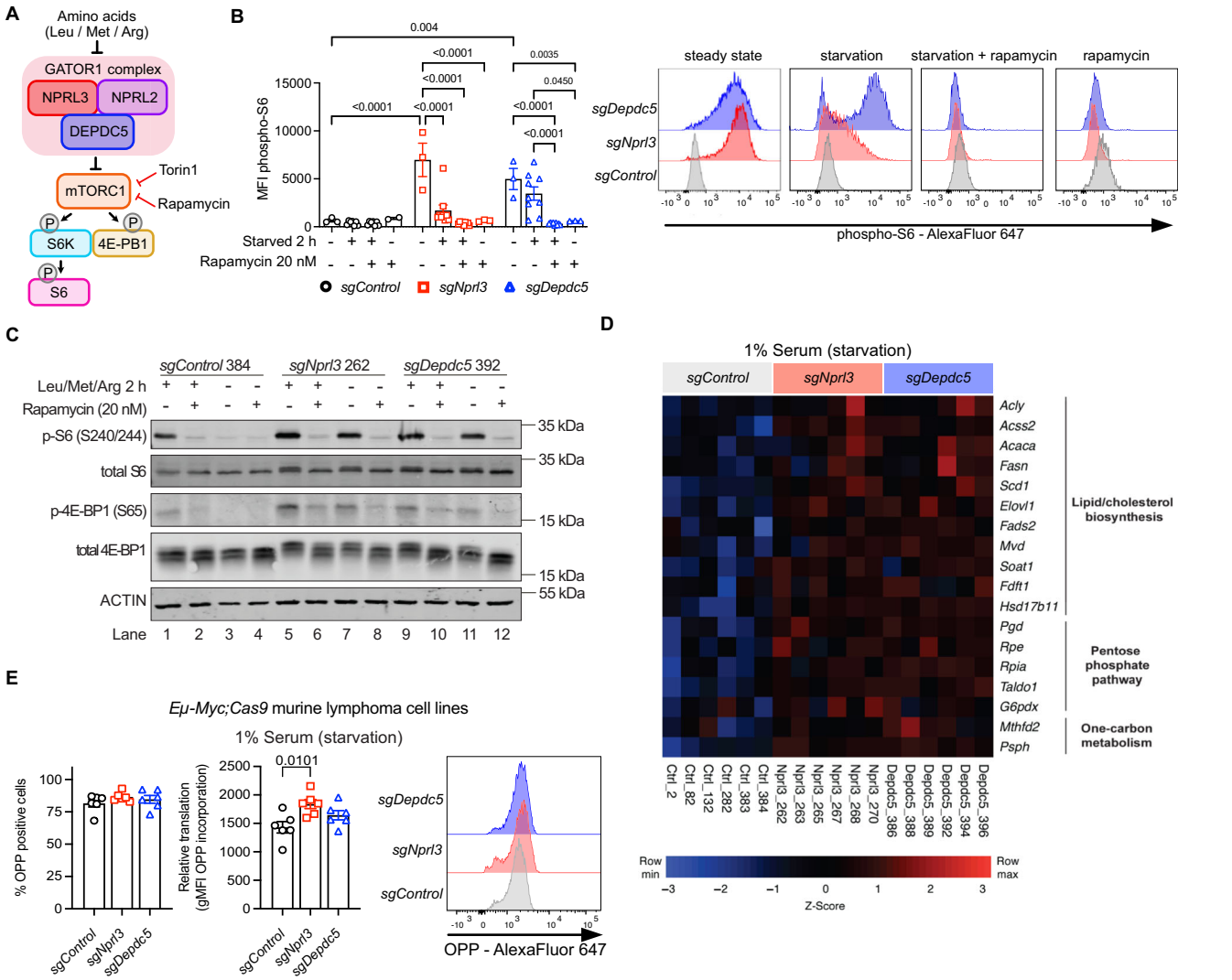

Fig. 4 | GATOR1 deficient lymphomas display alterations in mTORC1 regulated metabolic pathways. A Schematic of the GATOR1 complex that negatively regulates mTORC1 signaling in response to the availability of the amino acids leucine (Leu), methionine (Met) and arginine (Arg). mTORC1 can be directly inhibited by rapamycin or the mTORC1/mTORC2 inhibitor Torin1. **B** Phospho-S6 (activated S6) protein levels (presented as geometric mean fluorescence intensity = MFI) as measured by intracellular flow cytometry of *sgControl*, *sgNprl3* and *sgDepdc5* Eμ-*Myc;Cas9* lymphoma cell lines cultured at steady state (medium replete with amino acids and serum) or 2 h starvation (medium deprived of all amino acids and serum), and with or without treatment with rapamycin (20 nM). Summary graph of phospho-S6 protein levels in $n = 2$ *sgControl* and 3 of each *sgNprl3* or *sgDepdc5* lymphoma cell lines across three replicate experiments. Data are presented as mean values ± SEM. Representative flow cytometry histograms shown, from one lymphoma cell line per genotype. Flow cytometry gating strategy represented in Supplementary Fig. S8C. Two-way ANOVA statistical test with Tukey's multiple comparisons, significant *P* values displayed. **C** Western blot analysis of total S6, phospho-S6 (activated S6), total 4E-BP1 and phospho-4E-BP1 (inactivated 4E-BP1) proteins in *sgControl*, *sgNprl3* and *sgDepdc5* Eμ-*Myc;Cas9* lymphoma cell lines at steady state or after 2 h deprivation of Leu, Met and Arg, with and without treatment with rapamycin (20 nM) for 2 h, $n = 1$. Probing for ACTIN served as a protein loading control. Protein sizes are indicated in kDa. Uncropped Western blot images are provided as Source Data. **D** Heatmap of expression of genes involved in mTORC1-regulated metabolic pathways, derived from RNA-Seq analysis of *sgControl* ($n = 6$), *sgNprl3* ($n = 6$) and *sgDepdc5* ($n = 6$) Eμ-*Myc;Cas9* lymphoma cell lines after culture in medium containing 1% serum (i.e., starvation) for 24 h. Gene expression values are shown as Z-scores. **E** Relative protein translation was measured in negative control *sgControl*, *sgDepdc5* and *sgNprl3* Eμ-*Myc;Cas9* lymphoma cell lines after growth for 24 h in starvation medium containing 1% serum by monitoring incorporation of O-propargyl-puromycin (OPP). Flow cytometry gating strategy represented in Supplementary Fig. S8D. $n = 6$ independent lymphoma cell lines per genotype, 1-2 technical replicates. Data are presented as mean value ± SEM. Ordinary one-way ANOVA statistical test was used for comparison, significant *P* values displayed. Source data are provided as a Source Data file.

could translate into a meaningful therapeutic response in vivo. To this end, sg*Control* or GATOR1-deficient lymphoma cell lines were transplanted into RAG1-deficient mice which were then treated with rapamycin or vehicle (control) for five consecutive days (Fig. 5C). RAG1-deficient mice, lacking B and T cells, were used as recipients to prevent rejection of the lymphoma cells expressing immunogenic Cas9-eGFP protein. Remarkably, most RAG1-deficient mice transplanted with GATOR1-deficient lymphomas (lacking either *Nprl3* or *Depdc5*) were cured by rapamycin single agent treatment, whereas control lymphomas showed no response, with all recipients presenting with severe malignant disease within 30 days (Fig. 5D). These results demonstrate that GATOR1 deficiency causes addiction of Myc-driven lymphoma cells to excess mTORC1 signaling, rendering them vulnerable to single agent treatment with mTORC1 inhibitors.

Discussion

CRISPR gene knockout screens are a powerful approach to identify critical regulators of biological processes of interest[49,50], such as tumor

https://doi.org/10.1038/s41467-025-62615-y

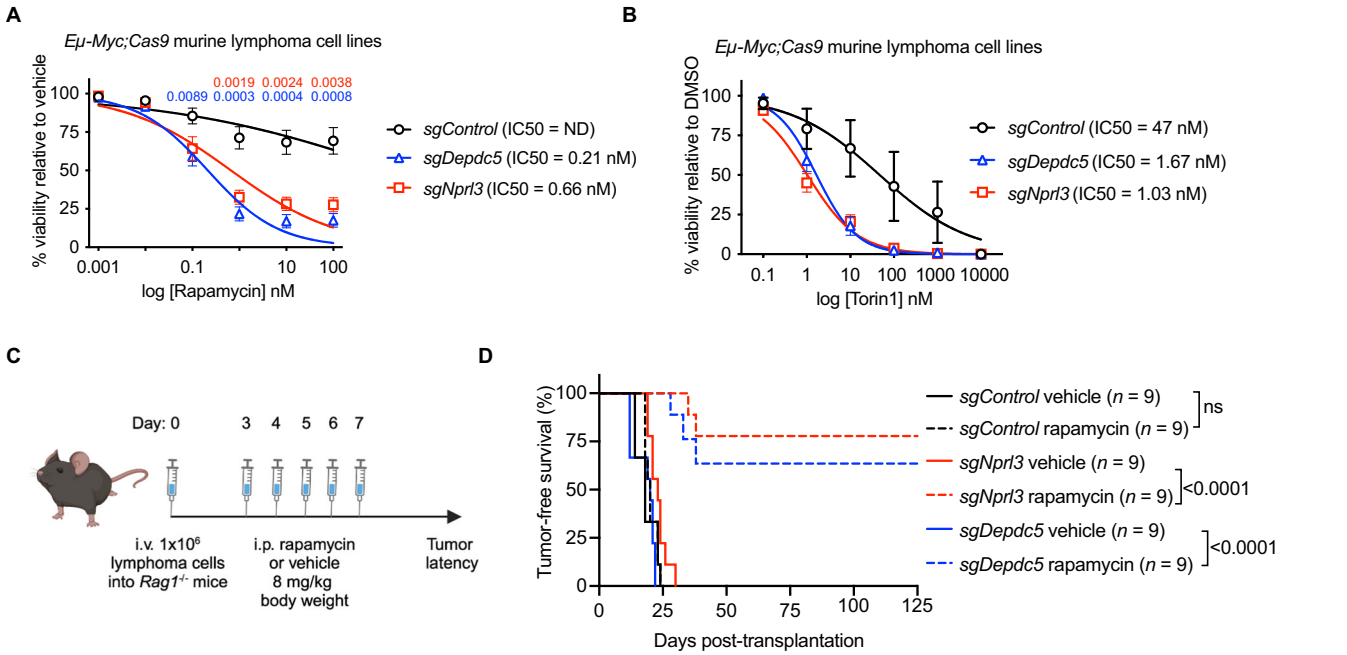

Fig. 5 | GATOR1 deficient lymphoma cells are highly sensitive to mTORC1 inhibition in vitro and in vivo. A, **B** Response curves of *sgControl*, *sgNprl3* or *sgDepdc5* Eμ-*Myc;Cas9* lymphoma cell lines to treatment in vitro with increasing doses of rapamycin (**A**) or Torin1 (**B**). Lymphoma cell viability was measured after 24 h of treatment with drug or vehicle by staining with Annexin V plus PI followed by flow cytometric analysis. Annexin V/PI double negative cells were deemed viable. Flow cytometry gating strategy represented in Supplementary Fig. S8B. $n = 3$ *sgControl* and 6 of each *sgNprl3, sgDepdc5* or *sgNprl2* lymphoma cell lines per genotype across 3 technical replicates. Data are presented as mean ± SEM, log transformed and fitting to non-linear regression. IC50 values are shown in brackets. Two-way ANOVA with Dunnett's multiple comparison statistical test used to compare dose response to *sgControl*, significant *P* values displayed in corresponding color per genotype. **C** Schematic of in vivo rapamycin treatment experiments. One million *sgControl*, *sgNprl3* or *sgDepdc5* Eμ-*Myc;Cas9* lymphoma cells were transplanted i.v. into the tail vein of RAG1-deficient mice, which lack B and T cells, to prevent lymphoma rejection due to an immune response against Cas9 and/or eGFP. Two days later, mice were randomly assigned into treatment arms, receiving either rapamycin at a dose of 8 mg/kg of body weight for 5 consecutive days by i.p. injection or vehicle as a control. Mice were monitored for lymphoma growth. Schematic created in BioRender. Potts, M. (https://BioRender.com/16f33zs). **D** Tumor-free survival curve of RAG1-deficient mice that had been transplanted with 1×10^6 negative control (*sgControl*), *sgNprl3* or *sgDepdc5* Eμ-*Myc;Cas9* lymphoma cell lines. $n = 9$ mice per treatment arm, with three cell lines per genotype, each injected into three recipient mice. Two-sided log-rank (Mantel-Cox) statistical test for survival curve comparison. Source data are provided as a Source Data file.

suppression. While some in vivo CRISPR screens have been conducted in mice[6,10,51–53], our screen differs by employing primary non-malignant cells (HSPCs from the fetal livers of Eμ-*Myc;Cas9* embryos) that can reconstitute the entire hematopoietic compartment and give rise to pre-B/B cell lymphomas when transplanted into lethally irradiated recipients. Maintaining coverage of a genome-wide sgRNA library in vivo is challenging due to several bottle neck events, such as loss of cells during transplantation or engraftment[14]. However, we detected sgRNAs targeting > 75% of all genes in vivo through sequencing gDNA from total spleen cells, comprising not only donor derived lymphoma cells but also donor derived non-malignant hematopoietic cells. While reasonably good coverage of sgRNAs were maintained in vivo, the design of our screen is limited by the number of hits that can be identified. This is due to using the Eμ-*Myc* mouse model, which develops monoclonal lymphoma, resulting in one hit being identified in the lymphoma per recipient mouse. Additionally, loss of p53 is such a strong driver of lymphoma development in this model that its sgRNAs will be overrepresented as a hit, outcompeting sgRNAs targeting other tumor suppressor genes. Nonetheless and importantly, several hits found in the lymphomas, representing known and previously unknown candidate tumor suppressors, were identified in our screen and individually validated to suppress Myc-driven lymphomagenesis. The success of this screen indicates that this approach can be applied to other biological questions, such as identifying unknown suppressors of tumorigenesis driven by different oncogenic lesions. This may even be achieved in non-hematopoietic cell types, as long as they are amenable to sgRNA library transduction and transplantation into the relevant tissue (e.g., transduction of mammary epithelial stem cells with a sgRNA library followed by their transplantation into cleared mammary fat pads of mice).

Here, by employing the highly efficient CRISPR/Cas9 gene knockout system in primary HSPCs from fetal livers using an unbiased genome-wide sgRNA library screen, we reveal genes encoding negative regulators of mTORC1 as potent tumor suppressor genes in Myc-driven lymphomagenesis. Modified cellular metabolism is a hallmark of cancer[54], and abnormalities in the expression of Myc or other factors regulating various metabolic pathways are known to cooperate during cancer development[2]. Genetic aberrations acting upstream of mTORC1, resulting in its constitutive activity, are frequent in many cancers. This includes activating mutations in AKT or loss of function mutations in TSC1 or TSC2, the latter both being hits in our screen. Notably, our screen revealed previously unknown suppressors of Myc-driven tumorigenesis that also function in the mTORC1 inhibitory pathway, namely the GATOR1 complex subunits (NPRL3, DEPDC5 and NPRL2). Loss of either proteins released negative regulation of mTORC1 and exerted as powerful impact on Myc-driven lymphoma development as loss of p53. This is similarly reflected in human lymphoma where low levels of GATOR1 component mRNAs are predictive of poorer survival in patients with B cell lymphoma, representing a precision oncology opportunity to further investigate. Defects in the p53 pathway are frequently selected for during lymphomagenesis in Eμ-*Myc* mice[20,23]. However, mutations in the GATOR1 complex subunits and p53 were mutually exclusive in our murine lymphoma model and in human DLBCL. This finding is consistent with other reports where aberrant mTORC1 activation during Myc-driven lymphomagenesis through loss of TSC2 or constitutive AKT expression obviated the

pressure to lose p53 pathway function[36,55]. Together these findings indicate that factors inhibiting mTORC1 activity are potent suppressors of Myc-driven lymphoma development and obviate the pressure to lose p53 function, and that such abnormalities are associated with poor prognosis in patients.

Previous reports show that abnormally elevated mTORC1 signaling in the absence of TSC2 or oncogenic AKT signaling contribute to lymphomagenesis primarily by inhibiting apoptotic cell death. Specifically, the increased mTORC1 regulation of protein translation resulted in higher levels of the pro-survival BCL-2 family member MCL-1, enabling escape from apoptotic cell death during malignant transformation[36]. In contrast, our results suggest loss of GATOR1 inhibition of mTORC1 activity promotes lymphomagenesis through enhanced cellular metabolism, supported by RNA-Seq and functional metabolic assays. However, while transcriptomic data provide valuable insight into global gene expression changes in metabolic pathways regulated by mTORC1, they do not capture mTORC1 driven effects on translation and protein synthesis. While both TSC2 and GATOR1 are potent inhibitors of mTORC1, they are activated through distinct mechanisms: GATOR1 is induced in response to amino acid deprivation, whereas TSC2 is regulated by multiple signaling cascades[27]. Notably, GATOR1 has not previously been implicated as a tumor suppressor in Myc-driven lymphomagenesis. This finding contributes to the expanding landscape of targetable vulnerabilities in this disease context. Our results highlight the nuanced differences in cancer dependencies that can emerge when distinct upstream alterations converge on a shared signaling pathway.

Methods

Ethics statement

The care and use of experimental mice were approved by and conducted according to the guidelines from The Walter and Eliza Hall Institute (WEHI) Animal Ethics Committee. Animal welfare was monitored by experienced animal technicians blinded to the type of fetal liver cells (FLCs) that irradiated mice had been transplanted with. Animals were housed in facilities with stabilized environment with 12-hour light/dark cycles. Water and chow (Barastoc, 8720610) were provided ad libitum.

Animal husbandry and mouse models

C57BL/6-Ly5.2, C57BL/6-Ly5.1 and *Rag1*/J knockout mice were obtained from the WEHI breeding facility (Kew, Victoria, Australia). *Eμ-Myc* transgenic[3] and constitutive *Cas9-eGFP* transgenic mice (a gift from Prof K.Rajewsky)[56] mice were maintained on a C57BL/6-Ly5.2 background. Sex was not considered in this study except that only male irradiated recipient mice were transplanted with FLCs from both male and female embryos to prevent anti-male antigen immune responses.

Lentiviral constructs and sgRNAs

A positive control sgRNA targeting *p53* (5′-GGCAACTATGGCTT CCACCT) and a negative control sgRNA targeting human *BIM* (5′-GCCCAAGAGTTGCGGCGTAT) were derived from the constitutive sgRNA FUGW expression vector[13]. The genome-wide mouse lentiviral CRISPR sgRNA library used for in vivo screening experiments, YUSA v1 was a gift from Kosuke Yusa (Addgene #50947)[28]. Two independent sgRNAs for in vivo validation experiments of hits and a negative control sgRNA targeting human *NLRC5*, (Supplementary Table 2) were obtained from the Merck CRISPR glycerol stock arrayed mouse sgRNA library available at WEHI (Sigma Aldrich #MSANGERG).

Lentivirus production

Lentiviruses were produced by transient transfection of HEK293T cells in 10 cm^2 dishes with 10 μg of vector DNA and packaging lentiviral constructs pMDL (5 μg), RSV (2.5 μg), and pENV (5 μg) using an established calcium phosphate precipitation method[57]. Viral supernatants were collected 48-72 h after transfection and passed through a 0.45 μm filter prior to transduction of cells.

Genotyping

Mouse genotypes were determined by PCR analysis of DNA derived from ear-clips or embryonic tails using direct tail lysis buffer (Viagen Biotech) and Proteinase K. Mastermix was prepared with GoTaq green (Promega, M7123) containing primers (final concentration 0.5 pmol/mL) with the addition of 1 μL total DNA. PCR cycling conditions were: 94 °C 4 min followed by 30 cycles (94 °C for 40 sec, 55 °C for 30 sec, 72 °C for 60 sec) and finally 72 °C for 5 min. PCR products were separated by gel electrophoresis on 2% DNA grade agarose (Bioline) gels in TAE buffer (40 mM Tris Acetate, 1 mM EDTA pH 8.0) containing ethidium bromide (0.2 μg/mL, Sigma) and imaged on the GelDoc DOCTM XR+ Gel Documentation system (Bio-Rad). PCR oligonucleotide primers (Integrated DNA Technologies) and expected products were as follows:

Eμ-Myc: expected band size ~900 bp
myc-1: 5′ -CAGCTGGCGTAATAGCGAAGAG
myc-2: 5′ -CTGTGACTGGTGAGTACTCAACC
Cas9-eGFP: expected band size of knock-in ~112 bp and wt ~196 bp
R26F2: 5′- GCCTCCTGGCTTCTGAGGACCG
R26R2: 5′- TCTGTGGGAAGTCTTGTCCCTCC
SAR: 5′-CCTGGACTACTGCGCCCTACAGA

Transduction of fetal liver cells and transplantation into lethally irradiated recipient mice

Embryonic day E13.5 FLCs were collected from *Eμ-Myc*;*Cas9* doubly transgenic mice (both transgenes in a heterozygous state in all experiments) on a C57BL/6-Ly5.2 background, and frozen in 90% fetal bovine serum (FBS)/10% DMSO (v/v). FLCs were thawed and cultured in alpha-minimum essential medium (α-MEM) GlutaMAX (Gibco, 35050061) supplemented with 10% FBS (Gibco), 1 mM L-glutamine (Gibco, 25030149), 1 mM sodium pyruvate (Gibco, 11360070), 100 U/mL penicillin-100 μg/mL streptomycin (Gibco, 15140122), 10 mM HEPES (Gibco, 15630080), 50 μM β-mercapto-ethanol and recombinant cytokines (see below) for 48 h prior to lentiviral transduction. The cytokines IL-6 (10 ng/mL), mouse stem cell factor (100 ng/mL), thrombopoietin (50 ng/mL) and FLT-3 ligand (10 ng/mL) were kindly provided by Dr. Jian-Guo Zhang (WEHI). Lentiviral supernatants were generated as described above. 12-well non-tissue culture treated plates (Nunc) were coated overnight with retronectin solution (32 μg/mL in PBS, produced in-house) at 4°C followed by blocking with 2% bovine serum albumin solution (Sigma-Aldrich, A1595) in PBS at 37°C for 30 min prior to coating with viral supernatant. Viral particles were supplemented with 8 μg/mL polybrene and centrifuged at 1,363 x g for 2 h onto the retronectin coated plates. Supernatants were removed from the lentivirus coated plates and FLCs/HSPCs were then added to wells and incubated for 24 h. FLCs transduced with vectors encoding sgRNAs were collected and pooled per sgRNA, washed in PBS, filtered through a 100 μm mesh, and then injected into lethally irradiated (two doses of 5.5 Gy, 3 h apart) 7–8 week-old C57BL/6-Ly5.1 recipient mice. One fetal liver equivalent was injected into two recipient mice each (~2 −3 × 10^6 FLCs per recipient mouse). A small amount of transduced FLCs was kept in culture for 48 h and transduction efficiency, routinely ~20–30%, was determined by BFP tag expression by flow cytometric analysis. Tumor-free survival was defined as the time from transplantation to ethical endpoint, which was determined by an experienced animal research technician who was blinded to the nature of the FLCs used for transplantation of the irradiated recipient mice. At sacrifice, peripheral blood was collected and analyzed using an ADVIA hematology analyzer (Bayer). Hematopoietic tissues, including spleen, lymph nodes, thymus and bone marrow, were collected for downstream analysis. The pooled CRISPR screens represent 6 independent cohorts of recipient mice. Validation experiments represent 2

independent cohorts of recipient mice. Each hematopoietic reconstitution experiment had internal controls of the same pool of FLCs transduced with a negative control sgRNA (*sgControl*) to account for generational differences in the *Eμ-Myc* mouse colony and possible differences in hematopoietic reconstitution of lethally irradiated recipients between different experiments.

Lymphoma cell transplantation and in vivo drug treatment

For in vivo drug treatment, 1×10^6 *Eμ-Myc;Cas9* lymphoma cells (C57BL/6-Ly5.2) were resuspended in 200 μL sterile PBS and injected into 7–12 week-old sex-matched recipient *Rag1*$^{-/-}$ mice by intravenous (i.v.) tail vein injection. *Rag1*$^{-/-}$ mice were used as recipients to prevent rejection of lymphoma cells owing to an immune response against Cas9 and/or eGFP. After three days, lymphoma transplanted recipient mice were treated for five consecutive days with vehicle or 8 mg/kg body weight rapamycin (LC laboratories) by intra-peritoneal (i.p.) injection. Rapamycin was first dissolved in 100% ethanol, stored at −20°C and further diluted in vehicle, 5.2% PEG 400 and 5.2% Tween 80, immediately before use. Mouse survival time was defined as the time from lymphoma cell line injection until mice were sick and had to be euthanized according to our animal ethics guidelines. This was judged by an experienced animal technician who was blinded to the nature of the lymphomas in the tumor bearing mice and the treatment.

Next generation sequencing

To identify pooled CRISPR sgRNAs, genomic DNA was isolated from spleens of reconstituted lymphoma bearing mice (containing malignant and normal hematopoietic cells) using DNeasy Blood and Tissue Kit (Qiagen) according to the manufacturer's instructions. Integrated sgRNAs in each lymphoma sample were amplified from 100 ng of genomic DNA using GoTaq Green Master Mix (Promega) and indexing primers with unique overhangs[29]. Amplicons were pooled, cleaned up using AMPure XP beads (Beckman Coulter) and sequenced on Illumina NextSeq or MiSeq platform. Enriched sgRNAs per lymphoma were calculated by number of reads mapping to each sgRNA in the library as a proportion of the total number of reads within a lymphoma sample. To identify InDels or mutations in individual target genes, DNA was extracted from lymphoma derived cell lines as described above and PCR amplified using sgRNA specific primers (Supplementary Table 3, p53 primers[30]) and GoTaq Green Master Mix (Promega). PCR products were amplified a second time using indexing primers, pooled, purified using AMPure XP beads (Beckman Coulter) and sequenced on an Illumina MiSeq platform. Reads were aligned to wt reference sequences obtained from *Ensembl*.

Cell culture

HEK293T cells were cultured in DMEM medium supplemented with 10% FBS. Prior to virus production, HEK293T cells were cultured in DME Glutamax medium (Gibco) supplemented with 10% FBS and 25 mM HEPES. *Eμ-Myc;Cas9* lymphoma cell lines (also referred to as *Eμ-Myc* lymphoma cells in the text) derived from lymphoma burdened tissues of sgRNA-transduced FLC transplant recipient mice were maintained in FMA medium[58]. All cell lines were regularly verified as mycoplasma negative (MycoAlert mycoplasma detection kit; Lonza, LT07-118) and authenticated by STR profiling at the Australian Genome Research Facility.

Flow cytometric analysis

Immunophenotyping of lymphoma cells was performed on single cell suspensions of primary lymphoma tissue from sick mice or *Eμ-Myc;Cas9* lymphoma derived cell lines stained with fluorochrome-conjugated antibodies against B220 (RA3-6B2), IgM (5.1), IgD (11-26 C), T cell antigen receptor beta (TCRβ, H57-597) and CD19 (ID3) in PBS supplemented with 5% FBS and Fcg receptor block (2.4G2 hybridoma supernatant, WEHI). Donor derived cells were identified as Ly5.2$^+$, CAS9 expressing, i.e., eGFP positive and sgRNA expressing, i.e., CFP or BFP positive. Dead cells were stained using propidium iodide (PI) at a final concentration of 2 μg/mL or ViaDye Red (Cytek, SKU R7-60008) according to manufactures instructions and analyzed on a Fortessax20 flow cytometer (Becton Dickinson) or the Cytek Aurora. Flow cytometry gating is represented in Supplementary Fig. S8A.

In vitro drug treatment assays

To assess drug sensitivity of *Eμ-Myc;Cas9* lymphoma cells, 5×10^4 cells were plated in triplicate into 96-well flat-bottom plates. Cells were treated with rapamycin (Cell Signaling Technology, 9904), torin1 (Cell Signaling Technology, 14379), nutlin-3a (Cayman Chemical, 18585), etoposide (Ebewe Pharmaceuticals Ltd, A-4866) or the MCL-1 inhibitor S63845 (Active Biochem, 6044) at the indicated concentrations. Cell viability was assessed after 24 h of treatment by staining cells with 2 μg/mL propidium iodide (PI) and AnnexinV conjugated to Alexa Fluor 647 (produced in-house) followed by flow cytometric analysis using a Fortessax20 flow cytometer (Becton Dickinson), A total of 10,000 events were recorded per sample. Data were analyzed using FlowJo analysis software. Cell viability was normalized to control cells treated with an equivalent volume of vehicle, either dimethyl sulfide (DMSO), water or 100% ethanol. Flow cytometry gating is represented in Supplementary Fig. S8B.

Intracellular flow cytometric analysis for phosphorylated S6

To assess the levels of phosphorylated (i.e., activated) S6 (phosho-S6) by flow cytometry, lymphoma cells were washed in PBS then resuspended in either FMA medium or Hanks Balanced Salt Solution (HBSS), for starvation condition, without or with supplementation with 20 nM rapamycin and incubated for 2 h at 37°C in 10% CO_2. Cells were spun down and 1×10^5 cells were harvested, washed in PBS and stained with green fixable viability dye (Thermo Fisher Scientific). Cells were fixed for 1 h using the eBioscience™ Foxp3/Transcription Factor Staining Buffer Set (Thermo Fisher Scientific) and stained according to the manufacturer's instructions. The antibodies used were directed against phospho-S6 conjugated to Alexa Fluor 647 (Cell Signaling Technology, 4851). Cells were then analyzed on an LSR IIC flow cytometer (Becton Dickinson). Data were analyzed using FlowJo analysis software and are presented as geometric mean fluorescence intensity (MFI). Flow cytometry gating is represented in Supplementary Fig. S8C.

Western blotting

Total protein extracts were prepared from *Eμ-Myc;Cas9* lymphoma cell lines and primary lymphomas containing the indicated sgRNAs by lysis in RIPA buffer (50 mM Tris-HCl, 150 mM NaCl, 1% NP-40, 0.5% DOC, 0.1% SDS) containing complete protease inhibitor cocktail (Roche) and phosphatase inhibitor cocktail (PhosphoSTOP™, Roche). Protein concentration was determined by using the Bradford assay (Bio-Rad). Between 10 to 30 μg of protein were prepared in Laemmli buffer boiled for 5 min. Proteins sizes were separated by SDS-PAGE using NuPAGE 10% Bis-Tris 1.5 mm gels (Life Technologies). Proteins were then transferred onto nitrocellulose membranes (Life Technologies) using the iBlot2 membrane transfer system (Thermo Fisher Scientific). Membranes were incubated with the relevant primary antibodies and then the HRP-conjugated secondary antibodies, both listed in the Supplementary Table 4, diluted in PBS containing 10% bovine serum albumin with 0.1% Tween20. Luminata Forte Western horseradish peroxidase (HRP) substrate (Merck Millipore) was used for developing the signal and membranes were imaged and analyzed using the ChemiDoc Imaging System with ImageLab software (Bio-Rad). Cell lysates from the p53 mutant *Eμ-Myc* lymphoma cell line EMRK1172[59] served as a positive control and the p53 wt *Eμ-Myc* lymphoma cell line EMRK1184[60] served as a negative control for high levels of mutant p53 protein and p19^{ARF} protein. For Western blot detection of phosphorylated proteins in Fig. 4C, lymphoma cell lines were cultured for 2 h in FMA medium

supplemented with 10% dialyzed heat-inactivated FBS, or FMA medium lacking the amino acids leucine, methionine and arginine, supplemented with 10% dialyzed heat-inactivated FBS (starvation medium). Concurrently, these cells were treated with DMSO (vehicle) or 20 nM rapamycin (Cayman Chemical, 20022). Cells were washed with PBS and lysed in ice-cold RIPA buffer containing a protease inhibitor cocktail (Sigma-Aldrich, P8340) and phosphatase inhibitors (PhosSTOP, Roche, 4906837001). Proteins in lysates were resolved according to their molecular weight by SDS-PAGE and transferred onto a nitrocellulose membrane (see above) followed by immunoblotting. Membranes were probed with primary antibodies followed by IRDye secondary antibodies (see Supplementary Table 4). Membranes were developed using infrared imaging (LI-COR Odyssey CLx). Uncropped Western blot images are provided as Source data.

RNA-Seq

Lymphoma cells were cultured in FMA medium containing full serum (10% FBS / serum) or under starvation conditions (FMA medium containing 1% serum) for 24 h prior to harvesting. RNA was isolated from *Eμ-Myc;Cas9* lymphoma cells using a NucleoSpin RNA kit (Macherey-Nagel) following the manufacturer's instructions. The 3' libraries were sequenced with an Illumina NextSeq 500, with single-end 75 bp reads to a depth of 15 M reads per sample. FastQ files were trimmed using Cutadapt (v1.16) and mapped to the mouse reference genome (mm10 GRCm38) using HISAT2 (v2.1.0). Samtools (v1.4.1) was used to convert SAM files to BAM format and to sort BAM files. Counts were generated using featureCounts (v1.6.0). Filtering and normalization of data were carried out using edgeR (v3.16)[61] and differential gene expression analysis was carried out using limma-voom (v3.4.6) [62]. Multi-dimensional Scaling (MDS) plots were generated using the plotMDS function (limma), where distances between samples represent the leading fold change (i.e., root-mean-square of the greatest 500 $\log_2$-fold changes between a given pair of samples). Pathway enrichment analysis was carried out using clusterProfiler (v4.6.0)[63] and DOSE (v3.24.2)[64], and visualized using enrichplot (v1.18.3)[65]. Heatmaps were generated using pheatmap (v1.0.12)[66], with values scaled by row.

Lipogenesis assay

A previously described protocol, with minor modifications, was employed[67]. Briefly, *Eμ-Myc;Cas9* lymphoma cells grown in 6-well plates were spiked with 0.2 μCi/mL [1-^{14}C]-acetate (PerkinElmer; NEC084H001MC) for the final 4 h of the experimental period. Cells were pelleted and washed twice with PBS, before lysis in 150 μL 0.5% Triton X-100. Lipids were extracted with 500 μL 2:1 (v/v) chloroform/methanol followed by low-speed centrifugation for 20 min. 150 μL ^{14}C-labeled lipids from the denser organic fraction were combined with 4 mL OptiPhase HiSafe 3 liquid scintillation cocktail (PerkinElmer; 1200.437) and radio-labeling was quantified using a Tri-Carb 2910 TR Liquid Scintillation Analyzer (PerkinElmer). ^{14}C-acetate incorporation was normalized to cell number.

Seahorse mito stress test

Three of each *sgControl*, *sgNprl3* and *sgDepdc5 Eμ-Myc;Cas9* lymphoma cell lines were treated with 0.45 nM of rapamycin or vehicle (DMSO) for 3 h. Drug was then washed out and 1×10^5 cells were plated in 5 replicate wells for immediate analysis using the Mito Stress Test Kit (Agilent, 103015-100) according to the manufacturer's instructions and using the following drug concentrations: 1.5 μM oligomycin, 2.0 μM FCCP, 0.5 μM Rotenone/Antimycin A. Mitochondrial function was analyzed on the Seahorse XFe96 (Agilent) analyzer. Plots were prepared using GraphPad Prism software.

Puromycin incorporation assay to determine rate of translation

A previously described protocol, with minor modifications, was employed[68]. *Eμ-Myc* lymphoma cells grown in 6-well plates were spiked with 20 μM O-propargyl-puromycin (Thermo Fisher Scientific, C10459) for the final 30 min of the experimental period. Cells were pelleted and washed with PBS. Cells were then fixed with 3.7% paraformaldehyde for 20 min, followed by a 20 min permeabilization with 0.5% Triton-X. Cells were then stained using the Click-iTTM Plus Alexa FluorTM 647 Picolyl Azide Toolkit (Thermo Fisher Scientific, C10643) according to the manufacturer's instructions. Puromycin incorporation was analyzed using a LSR FortessaTM X-20 flow cytometer (BD Biosciences). Data were analyzed using FlowJo analysis software. OPP positive cells were gated on live cells and data are presented as geometric mean fluorescence intensity (gMFI). Flow cytometry gating is represented in Supplementary Fig. S8D.

Mutational co-occurrence analysis in human DLBCL

Data pertaining to mutations in *TP53 (referred to as p53)*, *DEPDC5* and *NPRL2* in human DLBCL samples were obtained from[43–45] and the TCGA database (https://www.cancer.gov/tcga). Waterfall plots were generated for the samples ($n = 73$) using the waterfall function of the GenVisR[69] R package. Fisher's exact test was used to test for significance of co-occurrence of mutations.

Human B cell lymphoma patient survival analysis

Gene expression profiles and clinical characteristics were obtained from human B cell lymphoma patient cohorts for survival analysis[39,70–77]. The mRNA expression levels for *NPRL2*, *NPRL3* and *DEPDC5* across samples were divided into quartiles. Samples were divided into quartiles by *GATOR1*-low group, defined as patients with *NPRL2* or *NPRL3*, or *DEPDC5* mRNA expression in the bottom quartile (Q4). *GATOR1*-high patient samples were in the top quartile (Q1). The Kaplan-Meier method was used to estimate the survival functions among patient groups, and the log-rank test was used to test the differences in the overall survival between the selected groups computed using the survminer R package (v0.4.9). Patient numbers and statistical differences are shown in Supplementary Table 1.

Statistics and reproducibility

GraphPad Prism software (v8) was used to plot two-sided log-rank Kaplan-Meier (Mantel-Cox) mouse survival curves. For comparing two groups, Student's *t*-test was used, and for comparing more than two groups multiple t-test or two-way ANOVA were performed, unless otherwise stated in the figure legends. Data are presented as mean ± standard error of the mean (SEM), unless otherwise stated in figure legends. Significance was deemed where *P* value is less than 0.05, ns = no significant difference. For the CRISPR screen, no statistical analysis was performed, exploratory analysis of the sgRNA counts as heatmaps and pie charts were plotted using R package 'ggplot' (v2_3.3.5), 'o' represents the number of observations of sgRNAs or genes. No statistical method was used to predetermine sample sizes. Only mice euthanized due to reasons other than lymphoma were excluded from survival analysis. Animal assignment to experimental groups was randomized. Experienced animal technicians monitored the mice and were blinded to the nature of the experiment. Only *p53* wt *sgControl Eμ-Myc;Cas9* lymphoma cell lines were used in in vivo transplantation assays and in vitro cell death assays using rapamycin, torin1 and the MCL-1 inhibitor.

Reporting summary

Further information on research design is available in the Nature Portfolio Reporting Summary linked to this article.

Data availability

The RNA-Seq data generated in this study have been deposited in the NCBI Gene Expression Omnibus repository under accession code GSE285351.The screening data are available in the Supplementary Information and Supplementary Data Files. We believe all necessary data have been made available, but if any additional data are desired by

a reader, they will be made available upon request to the corresponding author. Source data are provided with this paper.

References

1. Dang, C. V. MYC on the path to cancer. *Cell* **149**, 22–35 (2012).
2. Stine, Z. E., Walton, Z. E., Altman, B. J., Hsieh, A. L. & Dang, C. V. MYC, metabolism, and cancer. *Cancer Discov.* **5**, 1024–1039 (2015).
3. Adams, J. M. et al. The c-myc oncogene driven by immunoglobulin enhancers induces lymphoid malignancy in transgenic mice. *Nature* **318**, 533–538 (1985).
4. Langdon, W. Y., Harris, A. W., Cory, S. & Adams, J. M. The c-myc oncogene perturbs B lymphocyte development in E-mu-myc transgenic mice. *Cell* **47**, 11–18 (1986).
5. Harris, A. W. et al. The E mu-myc transgenic mouse. a model for high-incidence spontaneous lymphoma and leukemia of early B cells. *J. Exp. Med* **167**, 353–371 (1988).
6. Chow, R. D. & Chen, S. Cancer CRISPR screens in vivo. *Trends Cancer* **4**, 349–358 (2018).
7. Potts, M. A., McDonald, J. A., Sutherland, K. D. & Herold, M. J. Critical cancer vulnerabilities identified by unbiased CRISPR/Cas9 screens inform on efficient cancer Immunotherapy. *Eur. J. Immunol.* **50**, 1871–1884 (2020).
8. Heitink, L. et al. In vivo genome-editing screen identifies tumor suppressor genes that cooperate with Trp53 loss during mammary tumorigenesis. *Mol. Oncol.* **16**, 1119–1131 (2022).
9. Song, C. Q. et al. Genome-wide CRISPR screen identifies regulators of mitogen-activated protein kinase as suppressors of liver tumors in mice. *Gastroenterology* **152**, 1161–1173 e1161 (2017).
10. Xu, C. et al. piggyBac mediates efficient in vivo CRISPR library screening for tumorigenesis in mice. *Proc. Natl. Acad. Sci. USA* **114**, 722–727 (2017).
11. Katigbak, A. et al. A CRISPR/Cas9 functional screen identifies rare tumor suppressors. *Sci. Rep.* **6**, 38968 (2016).
12. Martinez, S. et al. In vivo CRISPR screens reveal SCAF1 and USP15 as drivers of pancreatic cancer. *Nat. Commun.* **15**, 5266 (2024).
13. Janic, A. et al. DNA repair processes are critical mediators of p53-dependent tumor suppression. *Nat. Med* **24**, 947–953 (2018).
14. Chen, S. et al. Genome-wide CRISPR screen in a mouse model of tumor growth and metastasis. *Cell* **160**, 1246–1260 (2015).
15. Kodama, M. et al. In vivo loss-of-function screens identify KPNB1 as a new druggable oncogene in epithelial ovarian cancer. *Proc. Natl. Acad. Sci. USA* **114**, E7301–E7310 (2017).
16. Braun, C. J. et al. Versatile in vivo regulation of tumor phenotypes by dCas9-mediated transcriptional perturbation. *Proc. Natl. Acad. Sci. USA* **113**, E3892–E3900 (2016).
17. Dai, M. et al. In vivo genome-wide CRISPR screen reveals breast cancer vulnerabilities and synergistic mTOR/Hippo targeted combination therapy. *Nat. Commun.* **12**, 3055 (2021).
18. Manguso, R. T. et al. In vivo CRISPR screening identifies Ptpn2 as a cancer immunotherapy target. *Nature* **547**, 413–418 (2017).
19. Eischen, C. M., Roussel, M. F., Korsmeyer, S. J. & Cleveland, J. L. Bax loss impairs Myc-induced apoptosis and circumvents the selection of p53 mutations during Myc-mediated lymphomagenesis. *Mol. Cell Biol.* **21**, 7653–7662 (2001).
20. Eischen, C. M., Weber, J. D., Roussel, M. F., Sherr, C. J. & Cleveland, J. L. Disruption of the ARF-Mdm2-p53 tumor suppressor pathway in Myc-induced lymphomagenesis. *Genes Dev.* **13**, 2658–2669 (1999).
21. Campbell, K. J. et al. Elevated Mcl-1 perturbs lymphopoiesis, promotes transformation of hematopoietic stem/progenitor cells, and enhances drug resistance. *Blood* **116**, 3197–3207 (2010).
22. Egle, A., Harris, A. W., Bouillet, P. & Cory, S. Bim is a suppressor of Myc-induced mouse B cell leukemia. *Proc. Natl. Acad. Sci. USA* **101**, 6164–6169 (2004).
23. Michalak, E. M. et al. Puma and to a lesser extent Noxa are suppressors of Myc-induced lymphomagenesis. *Cell Death Differ.* **16**, 684–696 (2009).
24. Valente, L. J. et al. p53 efficiently suppresses tumor development in the complete absence of its cell-cycle inhibitory and proapoptotic effectors p21, Puma, and Noxa. *Cell Rep.* **3**, 1339–1345 (2013).
25. Kelly, P. N., Grabow, S., Delbridge, A. R., Strasser, A. & Adams, J. M. Endogenous Bcl-xL is essential for Myc-driven lymphomagenesis in mice. *Blood* **118**, 6380–6386 (2011).
26. Strasser, A., Harris, A. W., Bath, M. L. & Cory, S. Novel primitive lymphoid tumours induced in transgenic mice by cooperation between myc and bcl-2. *Nature* **348**, 331–333 (1990).
27. Saxton, R. A. & Sabatini, D. M. mTOR signaling in growth, metabolism, and disease. *Cell* **168**, 960–976 (2017).
28. Koike-Yusa, H., Li, Y., Tan, E. P., Velasco-Herrera, M. D. C. & Yusa, K. Genome-wide recessive genetic screening in mammalian cells with a lentiviral CRISPR-guide RNA library. *Nat. Biotechnol.* **32**, 267–273 (2014).
29. Aubrey, B. J. et al. An inducible lentiviral guide RNA platform enables the identification of tumor-essential genes and tumor-promoting mutations in vivo. *Cell Rep.* **10**, 1422–1432 (2015).
30. Aubrey, B. J. et al. Mutant TRP53 exerts a target gene-selective dominant-negative effect to drive tumor development. *Genes Dev.* **32**, 1420–1429 (2018).
31. Pal, S. et al. A druggable addiction to de novo pyrimidine biosynthesis in diffuse midline glioma. *Cancer Cell* **40**, 957–972.e910 (2022).
32. Potts, M. A. et al. Deletion of the transcriptional regulator TFAP4 accelerates c-MYC-driven lymphomagenesis. *Cell Death Differ.* **30**, 1447–1456 (2023).
33. Huang da, W., Sherman, B. T. & Lempicki, R. A. Systematic and integrative analysis of large gene lists using DAVID bioinformatics resources. *Nat. Protoc.* **4**, 44–57 (2009).
34. Sherman, B. T. et al. DAVID: a web server for functional enrichment analysis and functional annotation of gene lists (2021 update). *Nucleic Acids Res* **50**, W216–w221 (2022).
35. Bar-Peled, L. et al. A Tumor suppressor complex with GAP activity for the Rag GTPases that signal amino acid sufficiency to mTORC1. *Science* **340**, 1100–1106 (2013).
36. Mills, J. R. et al. mTORC1 promotes survival through translational control of Mcl-1. *Proc. Natl. Acad. Sci. USA* **105**, 10853–10858 (2008).
37. Hartleben, G. et al. Tuberous sclerosis complex is required for tumor maintenance in MYC-driven Burkitt's lymphoma. *Embo J.* **37**, e98589 (2018).
38. Hughes, J. et al. Knockout of the epilepsy gene Depdc5 in mice causes severe embryonic dysmorphology with hyperactivity of mTORC1 signalling. *Sci. Rep.* **7**, 12618 (2017).
39. Lenz, G. et al. Stromal gene signatures in large-B-cell lymphomas. *N. Engl. J. Med* **359**, 2313–2323 (2008).
40. Schmitt, C. A., McCurrach, M. E., de Stanchina, E., Wallace-Brodeur, R. R. & Lowe, S. W. *INK4a/ARF* mutations accelerate lymphomagenesis and promote chemoresistance by disabling p53. *Genes Dev.* **13**, 2670–2677 (1999).
41. Vassilev, L. T. et al. In vivo activation of the p53 pathway by small-molecule antagonists of MDM2. *Science* **303**, 844–848 (2004).
42. Valente, L. J. et al. Therapeutic Response to Non-genotoxic Activation of p53 by Nutlin3a Is Driven by PUMA-Mediated Apoptosis in Lymphoma Cells. *Cell Rep.* **14**, 1858–1866 (2016).
43. Chapuy, B. et al. Molecular subtypes of diffuse large B cell lymphoma are associated with distinct pathogenic mechanisms and outcomes. *Nat. Med* **24**, 679–690 (2018).
44. Lohr, J. G. et al. Discovery and prioritization of somatic mutations in diffuse large B-cell lymphoma (DLBCL) by whole-exome sequencing. *Proc. Natl. Acad. Sci. USA* **109**, 3879–3884 (2012).

45. Morin, R. D. et al. Frequent mutation of histone-modifying genes in non-Hodgkin lymphoma. *Nature* **476**, 298–303 (2011).
46. Wolfson, R. L. & Sabatini, D. M. The dawn of the age of amino acid sensors for the mTORC1 pathway. *Cell Metab.* **26**, 301–309 (2017).
47. Kotschy, A. et al. The MCL1 inhibitor S63845 is tolerable and effective in diverse cancer models. *Nature* **538**, 477–482 (2016).
48. Thoreen, C. C. et al. An ATP-competitive mammalian target of rapamycin inhibitor reveals rapamycin-resistant functions of mTORC1. *J. Biol. Chem.* **284**, 8023–8032 (2009).
49. Shalem, O. et al. Genome-scale CRISPR-Cas9 knockout screening in human cells. *Science* **343**, 84–87 (2014).
50. Wang, T., Wei, J. J., Sabatini, D. M. & Lander, E. S. genetic screens in human cells using the CRISPR-Cas9 System. *Science* **343**, 80–84 (2014).
51. Dong, M. B. et al. Systematic immunotherapy target discovery using genome-scale in vivo CRISPR screens in CD8 T Cells. *Cell* **178**, 1189–1204.e1123 (2019).
52. Sutra Del Galy, A. et al. In vivo genome-wide CRISPR screens identify SOCS1 as intrinsic checkpoint of CD4(+) T(H)1 cell response. *Sci. Immunol.* **6**, eabe8219 (2021).
53. Wertz, M. H. et al. Genome-wide in vivo CNS screening identifies genes that modify CNS neuronal survival and mHTT toxicity. *Neuron* **106**, 76–89.e78 (2020).
54. Hanahan, D. & Weinberg, R. A. Hallmarks of cancer: the next generation. *Cell* **144**, 646–674 (2011).
55. Wendel, H.-G. et al. Survival signalling by Akt and eIF4E in oncogenesis and cancer therapy. *Nature* **428**, 332–337 (2004).
56. Chu, V. T. et al. Efficient generation of Rosa26 knock-in mice using CRISPR/Cas9 in C57BL/6 zygotes. *BMC Biotechnol.* **16**, 4 (2016).
57. Herold, M. J., van den Brandt, J., Seibler, J. & Reichardt, H. M. Inducible and reversible gene silencing by stable integration of an shRNA-encoding lentivirus in transgenic rats. *Proc. Natl. Acad. Sci. USA* **105**, 18507–18512 (2008).
58. Kelly, G. L. et al. Targeting of MCL-1 kills MYC-driven mouse and human lymphomas even when they bear mutations in p53. *Genes Dev.* **28**, 58–70 (2014).
59. Wang, Z. et al. The anti-cancer agent APR-246 can activate several programmed cell death processes to kill malignant cells. *Cell Death Differ.* **30**, 1033–1046 (2023).
60. Baell, J. B. et al. Inhibitors of histone acetyltransferases KAT6A/B induce senescence and arrest tumour growth. *Nature* **560**, 253–257 (2018).
61. Robinson, M. D., McCarthy, D. J. & Smyth, G. K. edgeR: a Bioconductor package for differential expression analysis of digital gene expression data. *Bioinformatics* **26**, 139–140 (2010).
62. Ritchie, M. E. et al. limma powers differential expression analyses for RNA-sequencing and microarray studies. *Nucleic Acids Res* **43**, e47 (2015).
63. Wu, T. et al. clusterProfiler 4.0: a universal enrichment tool for interpreting omics data. *Innov. (Camb.)* **2**, 100141 (2021).
64. Yu, G., Wang, L. G., Yan, G. R. & He, Q. Y. DOSE: an R/Bioconductor package for disease ontology semantic and enrichment analysis. *Bioinformatics* **31**, 608–609 (2015).
65. Yu, G. et al. *enrichplot: Visualization of Functional Enrichment Result*. https://doi.org/10.18129/B9.bioc.enrichplot, R package version 1.28.4, https://bioconductor.org/packages/enrichplot (2022).
66. Kolde, R. pheatmap: Pretty Heatmaps version 1.0.12 from CRAN. 10.32614/CRAN.package.pheatmap. https://rdrr.io/cran/pheatmap/ (2019).
67. Ricoult, S. J., Yecies, J. L., Ben-Sahra, I. & Manning, B. D. Oncogenic PI3K and K-Ras stimulate de novo lipid synthesis through mTORC1 and SREBP. *Oncogene* **35**, 1250–1260 (2016).
68. Pavlova, N. N. et al. Translation in amino-acid-poor environments is limited by tRNA(Gln) charging. *Elife* **9**, e62307 (2020).
69. Skidmore, Z. L. et al. GenVisR: genomic visualizations in R. *Bioinformatics* **32**, 3012–3014 (2016).
70. Dubois, S. et al. Biological and clinical relevance of associated genomic alterations in MYD88 L265P and non-L265P-mutated diffuse large B-cell lymphoma: analysis of 361 cases. *Clin. Cancer Res* **23**, 2232–2244 (2017).
71. Hummel, M. et al. A biologic definition of Burkitt's lymphoma from transcriptional and genomic profiling. *N. Engl. J. Med* **354**, 2419–2430 (2006).
72. Lacy, S. E. et al. Targeted sequencing in DLBCL, molecular subtypes, and outcomes: a Haematological Malignancy Research Network report. *Blood* **135**, 1759–1771 (2020).
73. Reddy, A. et al. Genetic and functional drivers of diffuse large B cell lymphoma. *Cell* **171**, 481–494.e415 (2017).
74. Schmitz, R. et al. Genetics and pathogenesis of diffuse large B-cell lymphoma. *N. Engl. J. Med* **378**, 1396–1407 (2018).
75. Sha, C. et al. Molecular high-grade B-cell lymphoma: defining a poor-risk group that requires different approaches to therapy. *J. Clin. Oncol.* **37**, 202–212 (2019).
76. Shaknovich, R. et al. DNA methylation signatures define molecular subtypes of diffuse large B-cell lymphoma. *Blood* **116**, e81–e89 (2010).
77. Visco, C. et al. Comprehensive gene expression profiling and immunohistochemical studies support application of immunophenotypic algorithm for molecular subtype classification in diffuse large B-cell lymphoma: a report from the International DLBCL Rituximab-CHOP consortium program study. *Leukemia* **26**, 2103–2113 (2012).

Acknowledgements

The authors thank all members of the Blood Cells and Blood Cancer Division at The Walter and Eliza Hall Institute (WEHI***)*** and the Genome Engineering and Cancer Modeling Program at the Olivia Newton-John Cancer Research Institute (ONJCRI) for their support, advice, and sharing of reagents; G. Siciliano and all Bioservices staff at WEHI for technical assistance with the in vivo experiments and animal husbandry; A. Aeslop and the Screening lab at WEHI for the glycerol stock sgRNAs for target validation. We thank B. Haley and K. Potts for their constructive feedback on the manuscript. This work was supported by grants and fellowships from the Australian National Health and Medical Research Council (NHMRC) (Project Grants 1159658,1186575 and 1145728 to M.J.H., 1143105 to M.J.H. and A.S., Ideas Grants 2002618 and 2001201 to G.L.K., 2004212 and 2012313 to K.K.B., Program Grant 1113133 to A.S. and Fellowships 1020363 to A.S., 2017971 to M.J.H., 1102742 to J.E.V.), the Cancer Council of Victoria (project grant 1147328 and 2021 Grant In Aid to M.J.H., 1052309 to A.S., 1147328 to G.L.K. and Venture Grant to M.J.H. and A.S.), Victorian Cancer Agency (MCRF Fellowship 17028 to G.L.K. and 17020 to K.K.B.), Phenomics Australia (to A.J.K. and M.J.H.) the estate of Anthony (Toni) Redstone OAM (A.S. and G.L.K.), the Craig Perkins Cancer Research Foundation (G.L.K.), the Dyson Bequest (G.L.K.), the Harry Secomb Trust (G.L.K.), the University of Melbourne Research Training scholarship (M.A.P.), the National Natural Science Foundation of China (82201923) (Y.D.), the Uehara Memorial Foundation and JSPS Grant-in-Aid for Research Activity Start-up 20K22854 (S.M.) and Public Promoting Association Asano Foundation for Studies on Medicine (S.M.). H.D.C. was supported by the Marian and E.H. Flack Fellowship. This work was made possible by operational infrastructure grants through the Australian Government Independent Research Institute Infrastructure Support Scheme (361646 and 9000220) and the Victorian State Government Operational Infrastructure Support Program.

Author contributions

M.J.H. and A.S. conceived and designed the study; S.M. and Y.D. conducted in vivo CRISPR screens, M.A.P. conducted validation experiments in vivo and in vitro with assistance from G.H. K.K.B. designed metabolic studies including RNA-Seq and metabolic assays with input

from M.J.H. and A.S. which S.V. and K.E.T. conducted and analyzed; G.G. conducted bioinformatic analysis of CRISPR screens and bioinformatic analysis of TCGA patient datasets with input from A.T.P.; S.S. G.S. and A.D.J. conducted survival analyses and p53 mutual exclusivity analysis in human lymphoma patient datasets; S.W. ran NGS; L.W. provided technical mouse support; G.P., A..H.W., D.K., Z.W., C.K., S.D., G.L.K., A.J.K., M.P., L.T., Y.L., W.S., J.E.V., M.J.G.M., H.D.C., E.J.L., provided reagents, expertise or technical assistance; M.A.P., S.M., Y.D., S.V., K.E.T., K.K.B., A.S. and M.J.H. analyzed and interpreted results; M.A.P., A.S. and M.J.H. drafted and edited the manuscript which was then edited by all authors.

Competing interests
The authors declare no conflicts of interest with respect to this work.

Additional information
Supplementary information The online version contains supplementary material available at https://doi.org/10.1038/s41467-025-62615-y.

Correspondence and requests for materials should be addressed to Andreas Strasser or Marco J. Herold.

Peer review information *Nature Communications* thanks Fried Zwartkruis and the other, anonymous, reviewer(s) for their contribution to the peer review of this work. A peer review file is available.

[1]The Walter and Eliza Hall Institute of Medical Research, Parkville, Australia. [2]Department of Medical Biology, University of Melbourne, Melbourne, Australia. [3]Olivia Newton-John Cancer Research Institute, Heidelberg, Victoria, Australia. [4]The State Key Laboratory of Pharmaceutical Biotechnology, Department of Hepatobiliary Surgery, The Affiliated Drum Tower Hospital of Nanjing University Medical School, School of Life Sciences, Nanjing University, Nanjing, China. [5]Peter MacCallum Cancer Centre, Melbourne, Victoria, Australia. [6]Sir Peter MacCallum Department of Oncology, The University of Melbourne, Parkville, Australia. [7]Department of Hematology-Oncology, National University Hospital and Cancer Science Institute of Singapore, National University of Singapore, Singapore, Singapore. [8]School of Cancer Medicine, La Trobe University, Heidelberg, Victoria, Australia. [9]Department of Biochemistry and Pharmacology, The University of Melbourne, Melbourne, Australia. [10]Present address: Division of Hematology and Oncology, Department of Medicine, Kyoto Prefectural University of Medicine, Kyoto, Japan. [11]Present address: Centre for Cancer Biology, University of South Australia and SA Pathology, Adelaide, South Australia, Australia. [12]Present address: Department of Biochemistry and Molecular Biology, Monash Biomedicine Discovery Institute, Monash University, 15 Innovation Walk, Clayton, Victoria, Australia. [13]Present address: School of Dentistry and Medical Sciences, Charles Sturt University, Wagga Wagga, New South Wales, Australia. [14]Present address: Department of Hepatobiliary Surgery, The First Affiliated Hospital of Anhui Medical University, Hefei, Anhui Province, China. [15]These authors contributed equally: Margaret A. Potts, Shinsuke Mizutani, Yexuan Deng. [16]These authors jointly supervised this work: Kristin K. Brown, Andreas Strasser, Marco J. Herold. ✉e-mail: strasser@wehi.edu.au; marco.herold@onjcri.org.au